Hindawi
Shock and Vibration
Volume 2019, Article ID 3956169, 10 pages
https://doi.org/10.1155/2019/3956169

Research Article

Effect of Surface Morphology on Dynamic Characteristics of Cam-Follower Oblique Impact System

Wangqun Deng,[1] Haibo Feng,[2,3] Jianjun Wang,[2] and Yongfeng Yang [2,4]

[1]*AECC Hunan Aviation Powerplant Research Institute, Zhuzhou 412002, China*
[2]*Institute of Vibration Engineering, Northwestern Polytechnical University, Xi'an 710072, China*
[3]*AECC Sichuan Gas Turbine Establishment, Mianyang 621000, China*
[4]*Key Laboratory of Vibration and Control of Aero-Propulsion System Ministry of Education, Northeastern University, Shenyang 110819, China*

Correspondence should be addressed to Yongfeng Yang; yyf@nwpu.edu.cn

Received 4 December 2018; Accepted 27 December 2018; Published 22 January 2019

Academic Editor: Francesco Franco

The effects of the fractal characteristics on the dynamic characteristics of the oblique impact system are studied via considering the normal contact stiffness with fractal dimension parameter of the microstructure of the interface in this paper. The normal distribution is used to describe the trend of contact line length. The effects of the position parameters and the scale parameters are analyzed. The simulation results show that the increasing of the interface roughness can make the system response more stable. The system response eventually evolves into chaos as the fractal dimension increases. The system response changes between quasiperiod and chaos affected by the contact line length with a normal random distribution.

1. Introduction

Mechanical systems are usually modeled as multibody systems with nonsmoothness. Typical examples are the vibration and noise produced in engines, impact print hammers, railway brakes, or chattering of machine tools. These effects are due to the nonsmooth characteristics such as impacts, clearances, intermittent contacts, dry friction, unbalances, crack, or a combination of these effects [1–5]. In nonsmooth systems, the time evolution of displacements and velocities is not requested to be smooth. Especially for the impact, the velocities are even allowed to undergo jump at certain time instances in order to fulfill the kinematical restrictions.

Cam-follower devices are very important in impacting systems and widely applied in actual engineering systems. The rotation of the cam at special constant speed provides the force to operate the follower. The most common example is the valve train of the internal combustion engine. The cam rotation imparts force through the follower to the engine valve, while a spring provides the restoring force necessary to maintain contact between the two components [6, 7].

The impact on the cam-follower is a typical oblique impact. By using nonsmooth dynamics, oblique impact on rough bodies with an unsymmetrical configuration can result in self-locking or "jam" at the sliding contact if the coefficient of friction is large enough [8]. It has been observed that, under the variation of the cam-follower system parameters, the responses may exhibit complex behaviors including bifurcations and chaos [9, 10]. For example, Zhang [11] designed a new experimental device to verify the vibration suppression of a cantilever beam bond with a piezoelectric actuator by an adaptive controller. Ding et al. [12, 13] investigated the convergence of the Galerkin method of an elastic beam resting on a nonlinear foundation with viscous damping subject to a moving concentrated load. Alzate [14, 15] shows that a sudden transition to chaos is observed in an experimental cam-follower by ignoring the tangential friction effect. Considering the effect of tangential friction, Sundar et al. [16] studied the linear response of a cam-follower. In addition, the normal contact stiffness is an important parameter affecting the dynamic characteristics of the contact between the cam and follower when considering the surface topography [17]. In traditional research, the stiffness of the impact system is

mostly studied as a deterministic linear or nonlinear stiffness. However, the mechanical roughness of the surface topography may affect the wear, friction, and contact deformation, which make the stiffness no longer determined [18]. Majumdar and Bhushan [19] found that the mechanical processing surface has self-similar fractal characteristics and proposed the contact fractal theory and the contact fractal model (MB model), which uses the fractal dimension D and the fractal dimension parameter G to characterize the mechanical roughness of the surface topography.

The contact of the cam-follower system consists of a round bar and a cam, which subject to the two intersecting cylindrical contact model. When the two parts contact, the contact surface is equivalent to an ellipse and the length of the contact line is equal to the length of the ellipse's long axis. During the operation of the cam-follower system, the length of contact line is constantly changing due to the continuous change of the contact force between the follower and cam. Therefore, the length of the contact line should be dynamically changed in the actual analysis.

The motivation of this paper is to establish the normal contact stiffness model based on the contact fractal theory via considering the fractal dimension D and the fractal dimension parameter G. Normal distribution will be used to describe the variation of the contact line length. The effects of the normal contact stiffness on the dynamic characteristics of the oblique impact system are studied.

2. Mechanical Model and Dynamic Equation

2.1. System Description. Figure 1 shows the schematic diagram of the cam-follower system. The follower makes a fixed axis rotation around O. The cam rotates around a fixed point O', R is the radius, and ω is the rotating angular velocity of the cam. The eccentric e is the distance between the geometric center C and the rotation point O'. The angular displacement of the cam is $\theta_c = \angle CO'x'$, and the angle between the follower and the horizontal axis is θ_f. At the initial time, A is the cam and follower contact point. When the system is rotating, B_f and B_c are the impact points on the follower and cam, respectively. iAj is a local coordinate system, and note δ_i as the distance $|\overrightarrow{B_f B_c}|$, which indicates the deformation of contact springs between the follower and cam. Obviously, the size of the δ_i can be used to determine whether the impact occurs or not, that is, $0 < \delta_i$ indicates the separate state, and $0 \geq \delta_i$ indicates the contact state.

2.2. The Equation of Motion. During the operation of the cam, the follower will show two kinds of motion states, namely, the contact state and the separate state, and the topology of the system will change with time.

Using the Lagrangian approach, the follower motion equation can be obtained:

$$\begin{cases} J\ddot{\theta}_f + \dfrac{mgl}{2}\cos(\theta_f) = 0, & \text{separate state,} \\ J\ddot{\theta}_f + \dfrac{mgl}{2}\cos(\theta_f) = F_n l_1 + \mu_f \operatorname{sgn}(v_r(t)) F_n, & \text{contact state,} \end{cases} \tag{1}$$

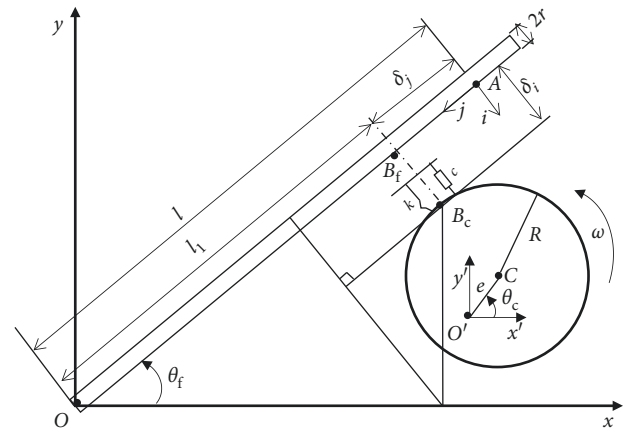

Figure 1: Schematic diagram of the cam-follower system.

where J is the follower's moment of inertia, μ_f is the friction factor between follower and cam, and F_n is the normal contact force, and the expression is

$$F_n(t) = -K_n\delta_i - c\dot{\delta}_i, \tag{2}$$

where K_n and c represent the equivalent stiffness and damping coefficient of the normal contact, respectively.

Using the pure damping model which was proposed by Padmanabhan [20], the given damping coefficient is

$$c = \beta K_n \delta_i, \tag{3}$$

where β is the impact damping factor.

2.3. Impact Law. In this model, the impact time is very short, the displacement of the various parts is constant, and the speed changes before and after the impact. By ignoring the plastic characteristic, the oblique impact problem studied here only involves the elastic impact. Considering the impact recovery coefficient, the impact process is divided into two stages: compression and recovery. The velocity relationship before and after the impact is

$$\dot{\theta}_f(t_i^+) = -\xi\dot{\theta}_f(t_i^-) + (1+\xi)\frac{-\dot{x}_{B_c}\sin(\theta_f) + \dot{y}_{B_c}\cos(\theta_f)}{l_1}, \tag{4}$$

where ξ is the coefficient of impact recovery and $\dot{x}_{B_c}$ and $\dot{y}_{B_c}$ are given by the following expressions:

$$\begin{cases} \dot{x}_{B_c} = -e\dot{\theta}_c\sin(\theta_c) - R\dot{\theta}_{f_c}\cos(\theta_{f_c}), \\ \dot{y}_{B_c} = e\dot{\theta}_c\cos(\theta_c) - R\dot{\theta}_{f_c}\sin(\theta_{f_c}). \end{cases} \tag{5}$$

2.4. Normal Contact Stiffness Fractal Model. The contact stiffness is related to the material properties of the two contacting objects and the geometry of the contact surface. For a specific mechanical system, the material properties of the components have been determined, and only the contact surface geometry may affect the contact stiffness coefficient.

The actual mechanical interface consists of two rough surfaces. According to the results of Reference [21], the

contact area can be reduced to a rigid plane in contact with a rough surface. Figure 2 shows a schematic diagram of the contact between a microconvex body and a rigid plane. When the contact occurs, the real area of the rough surface accounts for only a small part of the nominal contact area. Therefore, the contact problem of the mechanical joint surface can be handled with the contact of the convex body. When the surface is stressed, the microconvex body will occur elastic or plastic deformation. We focus on the elastic deformation of the local components.

The single microconvex body on the rough surface is equivalent to the sphere, and R is recorded as its equivalent radius of curvature.

When the normal load p is applied to the contact point, δ is the normal contact deformation. The radius of the contact area is R. According to Reference [20], the relationship between p and δ is

$$p = \frac{4}{3} E R^{1/2} \delta^{3/2}, \tag{6}$$

where E is the modulus of elasticity of the two contact materials:

$$\frac{1}{E} = \left[\frac{1 - \vartheta_f^2}{Y_f} + \frac{1 - \vartheta_c^2}{Y_c} \right], \tag{7}$$

where ϑ and Y represent Poisson's ratio and Young's modulus of the material, respectively. Subscripts f and c represent the follower and cam.

According to equation (6), the normal contact stiffness of a single microconvex body contact with a rigid plane is

$$k_n = 2ER^{1/2}\delta^{1/2}. \tag{8}$$

According to the geometric relationship between the microconvex deformation and the typical value of the fractal roughness parameter G in Reference [22], $R \gg \delta$, and the expression of the cross-sectional area a' of the microconvex body is

$$a' = 2\pi R\delta. \tag{9}$$

Substituting equation (9) into (8), we can obtain

$$k_n = 2E\sqrt{\frac{a'}{2\pi}}. \tag{10}$$

According to the contact fractal theory [23], the distribution function of the contact point of the microcontact area a' is

$$n(a') = \frac{D}{2} \frac{a_1'^{(D/2)}}{a'^{(D/2)+1}}, \tag{11}$$

$$a_1' = \frac{2 - D}{D} A_r, \tag{12}$$

where a_1' is the actual contact area of the maximum contact point, A_r is the real contact area of the rough surface, and D is the fractal dimension of rough surface which reflects the irregularity and complexity of surface profile on all scales. Considering the two-dimensional fractal problem, the range $D \in [1, 2]$. According to the Hertz contact theory, when contact occurs, the contact area of two objects is elliptical, and the real contact area A_r is about $10^{-5}\,m^2$.

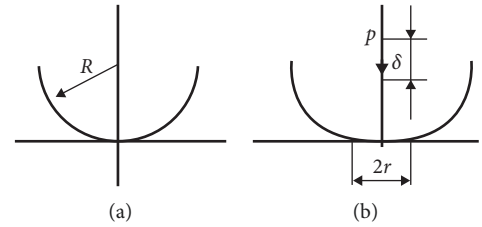

Figure 2: Schematic diagram of the contact between a microconvex body and a rigid plane. (a) Unloaded state. (b) Loaded state.

Assume that the rough surface is isotropic in the microtopography. According to the contact fractal theory, the microconvex body contact deformation belongs to the plastic deformation when $a' < a_c'$, and the contact deformation belongs to the elastic deformation when $a' > a_c'$. a_c' is determined by Reference [24] as

$$a_c' = \frac{G^2}{(k\varphi/2)^{(2/(D-1))}}, \tag{13}$$

where G is the fractal roughness parameter of the rough surface. Larger G means rougher contact surface. $k = H/\sigma_y$ is a factor related to the softer material hardness H and the yield strength σ_y, and k is generally taken as 2.8. $\varphi = \sigma_y/E$ is a factor related to σ_y and the equivalent elastic modulus E.

Thus the normal contact stiffness of the joint surface is

$$K_n = \int_{a_c'}^{a_1'} k_n n(a')\, da'. \tag{14}$$

Substituting Equations (10) and (11) into (14), we can obtain

$$K_n = \frac{2ED}{\sqrt{2\pi}(1 - D)} a_1'^{(D/2)} \left(a_1'^{((1-D)/2)} - a_c'^{((1-D)/2)} \right). \tag{15}$$

According to the relationship $a' = 2a$, we have

$$\begin{cases} a_1' = 2a_1, \\ a_c' = 2a_c. \end{cases} \tag{16}$$

Substituting Equation (16) into (15), the normal contact stiffness can be obtained

$$K_n = \frac{2ED}{\sqrt{\pi}(1 - D)} a_1^{D/2} \left(a_1^{((1-D)/2)} - a_c^{((1-D)/2)} \right). \tag{17}$$

For a definite rough surface, a_c is constant, and the normal stiffness depends on the real contact area a_1 of the maximum contact point.

2.5. Contact Line Length with Random Normal Distribution. Using the Hertz contact theory in Reference [24], the equivalent stiffness coefficient is given by

$$K_n = \frac{\pi}{4} E l_\lambda, \tag{18}$$

where l_λ represents the length of the contact line.

Assume that the length of the contact line obeys the law of normal distribution, that is, the contact line length is controlled by the position parameter μ and the scale parameter σ. μ and σ, respectively, determine the position and amplitude of the normal distribution. Figure 3 shows the

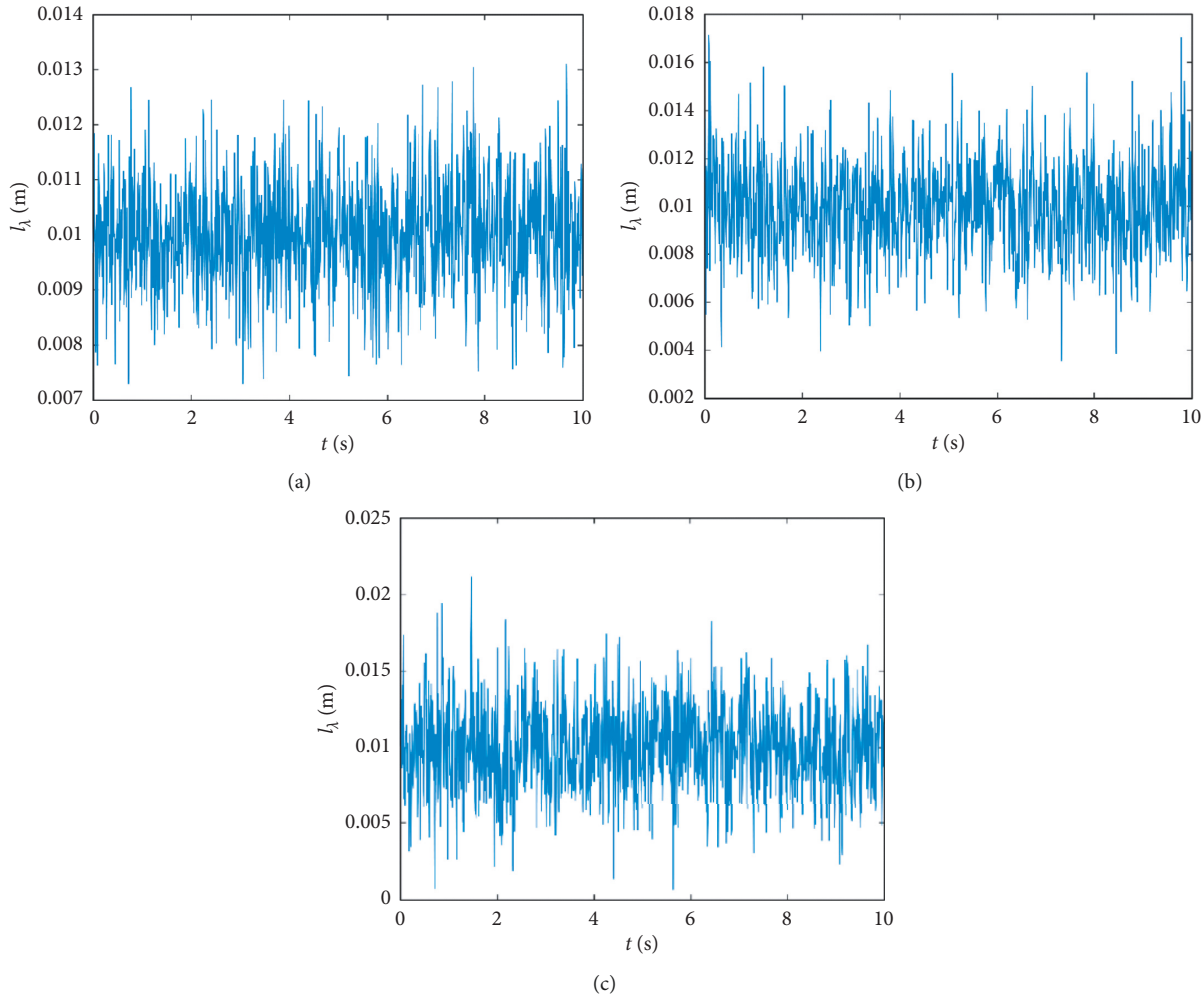

Figure 3: Normally distributed random contact line length. (a) $\mu = 0.01$ m, $\sigma = 0.001$ m. (b) $\mu = 0.01$ m, $\sigma = 0.002$ m. (c) $\mu = 0.01$ m, $\sigma = 0.003$ m.

numerical simulation of the normal contact line length with random distribution. It is found that the amplitude range of the contact line length increases as the scale parameter σ increases. Obviously, the position parameter μ and the scale parameter σ affect the dynamic response of the system. $\sigma = 0$ indicates that the normal contact line length is constant, and $\sigma \neq 0$ indicates that the length is a random parameter.

3. Numerical Simulation

Considering the system dynamic equations contain strong nonlinear time-varying parameters, the analytic solutions are difficult to obtain. The numerical iterative method, fourth-order Runge–Kutta, is employed to solve the dynamic equations and calculates the system's response over 20 seconds. From the numerical simulation results, it is found that the first several periods' responses are generally affected by the initial integral parameters and we give up these responses to eliminate the transient effect.

At the initial time, the follower and cam keep in touch, and the parameter values of the cam-follower oblique impact system are shown in Table 1. In the simulation process, the system response is calculated by equation (1), and the follower angular velocity value is calculated by the impact law of equation (4).

Table 1: Values of the system parameters.

Parameters	Values
Follower length, l	0.6 m
Follower radius, r	0.005 m
Follower mass, m	0.3676 kg
Cam radius, R	0.09 m
Cam eccentricity, e	0.04 m
Poisson's ratio, ϑ	0.3
Acceleration of gravity, g	9.81 m/s^2
Friction coefficient, μ_f	0.3
Impact damping factor, β	3.25 s/m
Impact recovery coefficient, ξ	0.42
Modulus of elasticity, Y	$2.07*10^{11}$ Pa
Cam speed, ω	28.7 rad/s

3.1. Effect of Contact Line Length. The length of the contact line affects the nonlinear stiffness coefficient of the contact

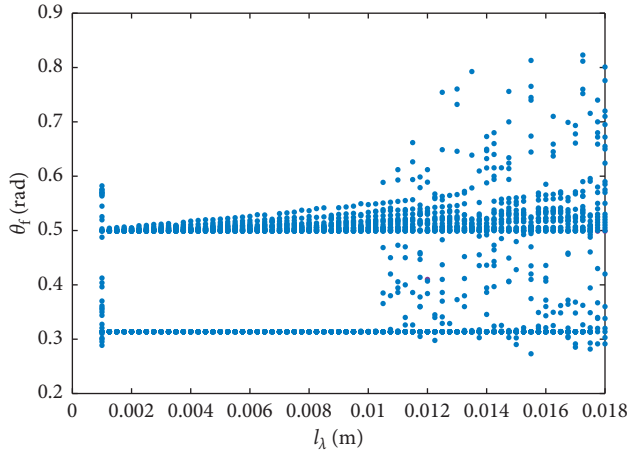

Figure 4: Global bifurcation diagram of θ_f.

surface. Taking the contact line length l_λ as the control parameter, l_λ varies from 0.001 m to 0.018 m in steps of 0.00025 m, and the global bifurcation diagram of the follower angle position θ_f is shown in Figure 4. It can be found from the bifurcation diagram that the cam-follower system exhibits complex dynamic behaviors, including periodic motion, quasiperiodic motion, and chaotic motion. The system response changes from the initial chaotic motion first to periodic 2, then to quasiperiod 2, and then finally to chaos.

3.2. Effect of Joint Surface Fractal. Take $k = 2.8$, $\varphi = 0.01$, $A_r = 10^{-5}$ m^2, $D \in [1.36, 1.56]$, and G takes 10^{-9} m, 10^{-10} m, and 10^{-11} m, respectively. Figure 5 shows the variation of contact stiffness K_n with fractal parameters G and D. It can be found that K_n increases with the increase of the fractal dimension D and decreases with the increase of the scale parameter G, which indicates that increasing the roughness of the joint surface is benefit to the reduction of the normal contact stiffness.

Taking the fractal dimension D as the control parameter, the global bifurcation diagram of the follower angle position θ_f for the different scale parameters G is shown in Figure 6. It can be found from Figure 6 that the system response is more sensitive to the fractal parameters D and G. Smaller parameter variety will affect the response state. When $G = 10^{-10}$ m, the system first enters the period 2, soon moves into the quasiperiod 2, and finally moves into large amplitude chaos. In addition, $G = 10^{-9}$ m corresponds to the larger bandwidth of the relatively stable response interval of the system. Smaller G means smaller joint normal contact stiffness, and it is benefit to the stability of the system response.

3.3. Effect of Random Contact Line Length. From the bifurcation diagram of Figure 4, it can be found that the system performs quasiperiod 2 motion when $l_\lambda = 0.008$ m. Figure 7 shows the system response with different contact line length distributions for $\sigma \in [0.001\text{ m}, 0.003\text{ m}]$ and $\mu = 0.008$ m. θ_{fc} is the angle between the rod and the horizontal direction in the persistent contact. It can be found that as the random deviation σ increases, the system response evolves from quasiperiodic to chaos, which indicates that the contact line length l_λ with a normal random distribution can lead the system unsteady.

In Figure 4, when $l_\lambda = 0.015$ m, the system response is chaos. Figure 8 shows the system response for different σ when $\mu = 0.015$ m and $l_\lambda = 0.015$ m. It can be seen that all systems exhibit quasiperiod 2 motions, which indicates that the random deviations can effectively suppress the chaos in the system.

The determinate response is shown in Figure 9 when $l_\lambda = 0.023$ m, and it is chaos. Figure 10 shows the system response after applying a random deviation when $\mu = 0.023$ m. It can be found that the system also exhibits quasiperiod 2, which means applying random deviation can effectively suppress the chaos in the system.

4. Conclusions

In this paper, the fractal model of the normal contact stiffness has been established by considering the micro-topography of the joint surface. The effects of the fractal dimension D and the scale parameter G on the dynamic characteristics of the cam-follower oblique impact system have been studied. The effects of the location and scale parameters of the system dynamic characteristics have been analyzed. The main conclusions can be listed as follows:

(1) Increasing the roughness of the joint surface is a benefit to the reduction of the normal contact stiffness.

(2) The system response is more sensitive to the fractal parameters, D and G. The response state

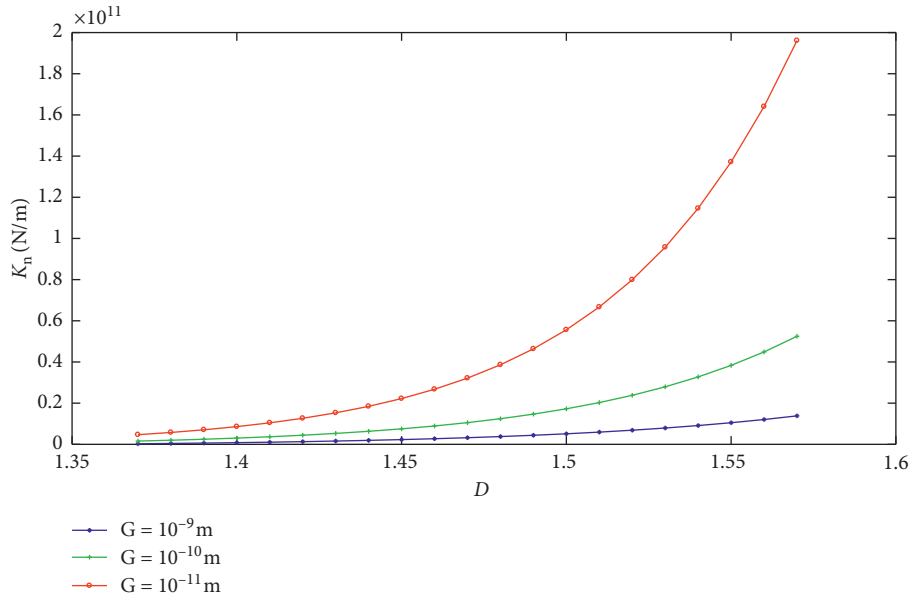

Figure 5: Variation of contact stiffness K_n with G and D.

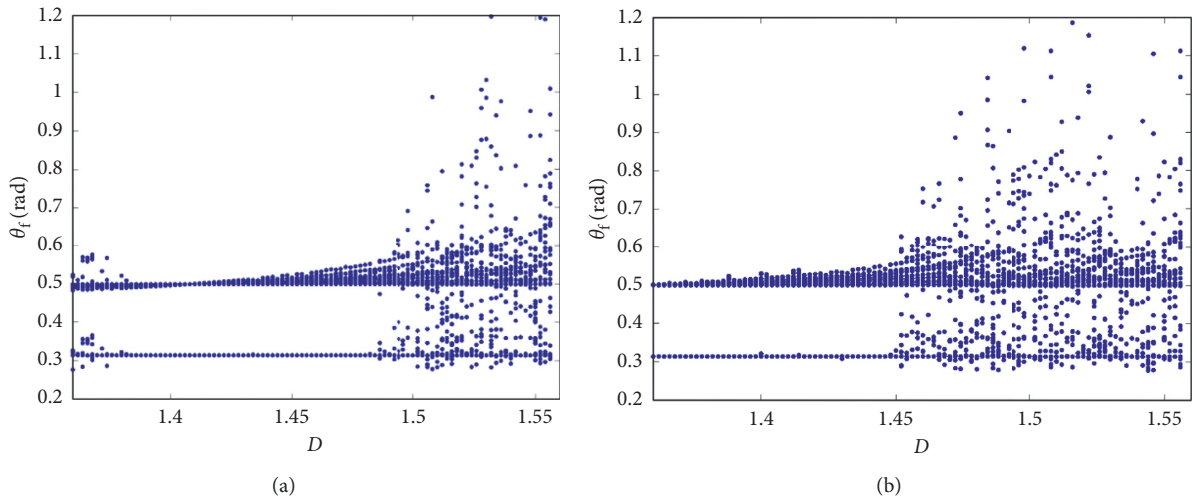

Figure 6: Global bifurcation diagram of θ_f with D for different G. (a) $G = 10^{-9}$ m. (b) $G = 10^{-10}$ m.

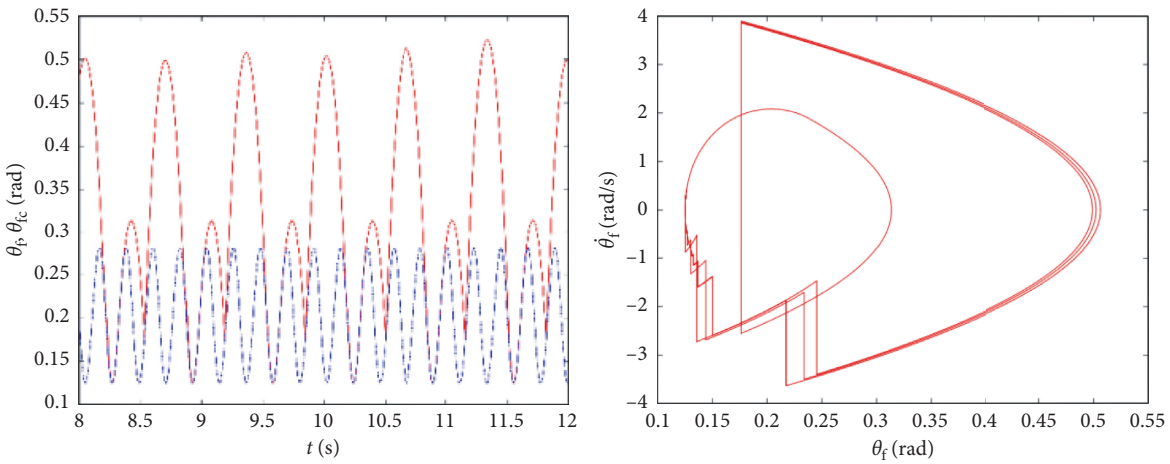

Figure 7: Continued.

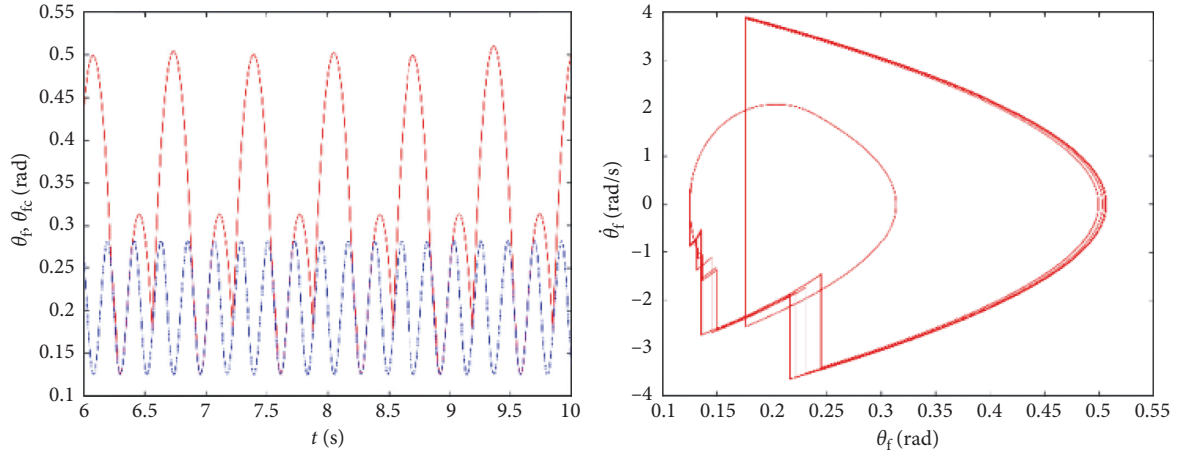

(b)

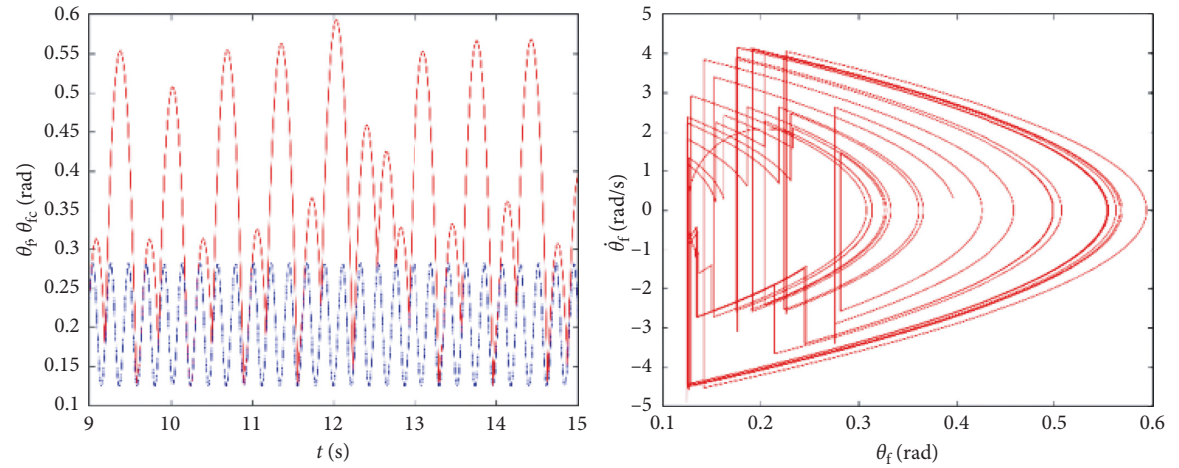

(c)

Figure 7: System response with different contact line length distributions (μ = 0.008 m). (a) Quasiperiod 2 (σ = 0.001 m; left frame: red represents θ_f, blue represents θ_{fc}). (b) Quasiperiod 2 (σ = 0.002 m; left frame: red represents θ_f, blue represents θ_{fc}). (c) Chaos (σ = 0.004 m; left frame: red represents θ_f, blue represents θ_{fc}).

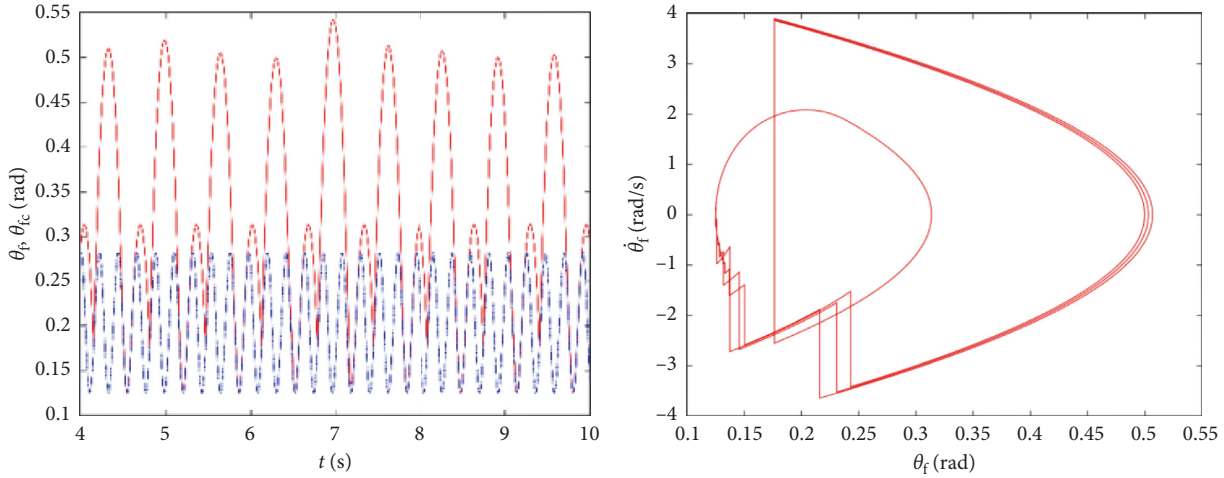

(a)

Figure 8: Continued.

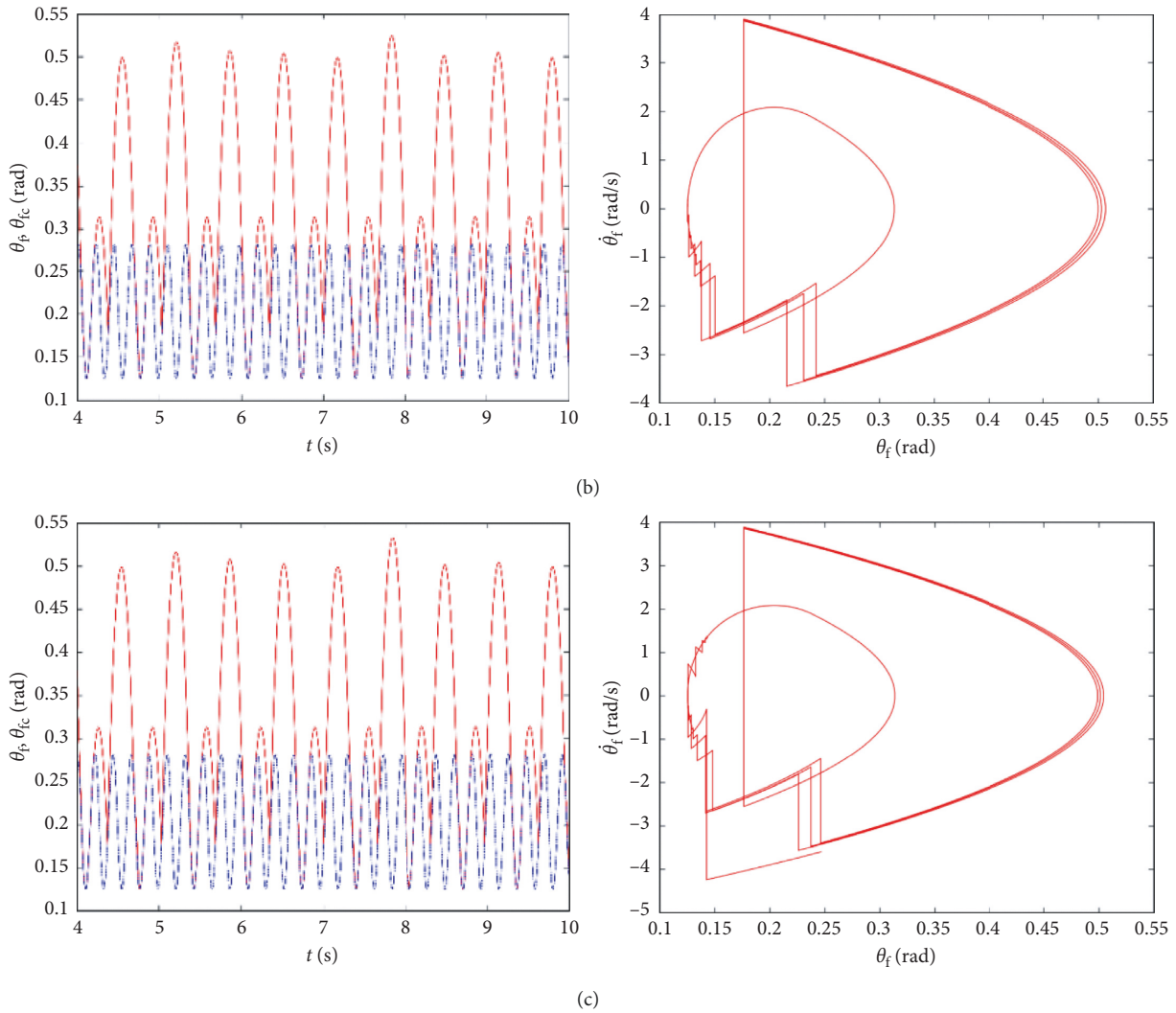

Figure 8: System response for the different σ ($\mu = 0.015$ m). (a) Quasiperiod 2 ($\sigma = 0.001$ m; left frame: red represents θ_f, blue represents θ_{fc}). (b) Quasiperiod 2 ($\sigma = 0.002$ m; left frame: red represents θ_f, blue represents θ_{fc}). (c) Quasiperiod 2 ($\sigma = 0.003$ m; left frame: red represents θ_f, blue represents θ_{fc}).

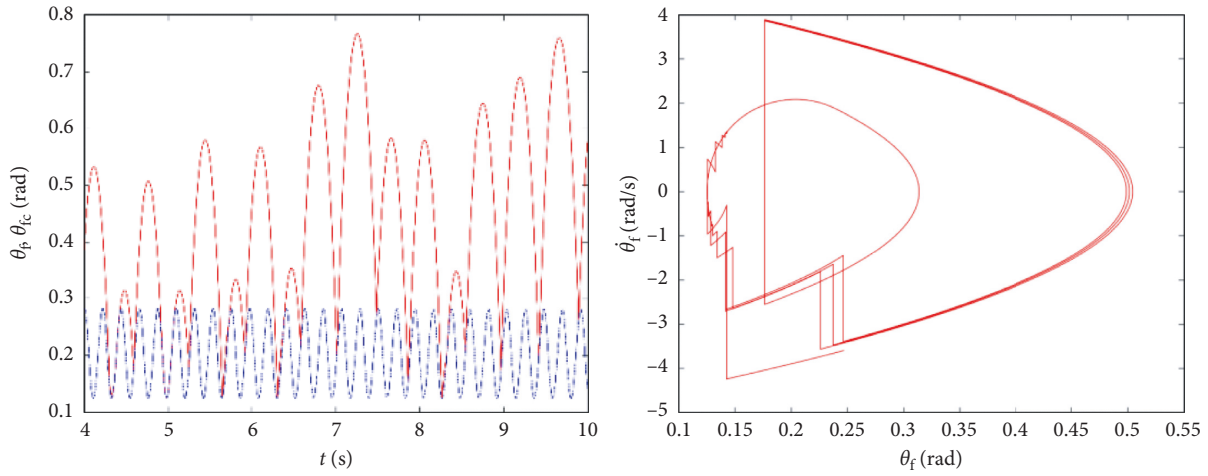

Figure 9: Chaotic response when $l_\lambda = 0.023$ m ($\mu = 0.023$ m, $\sigma = 0$).

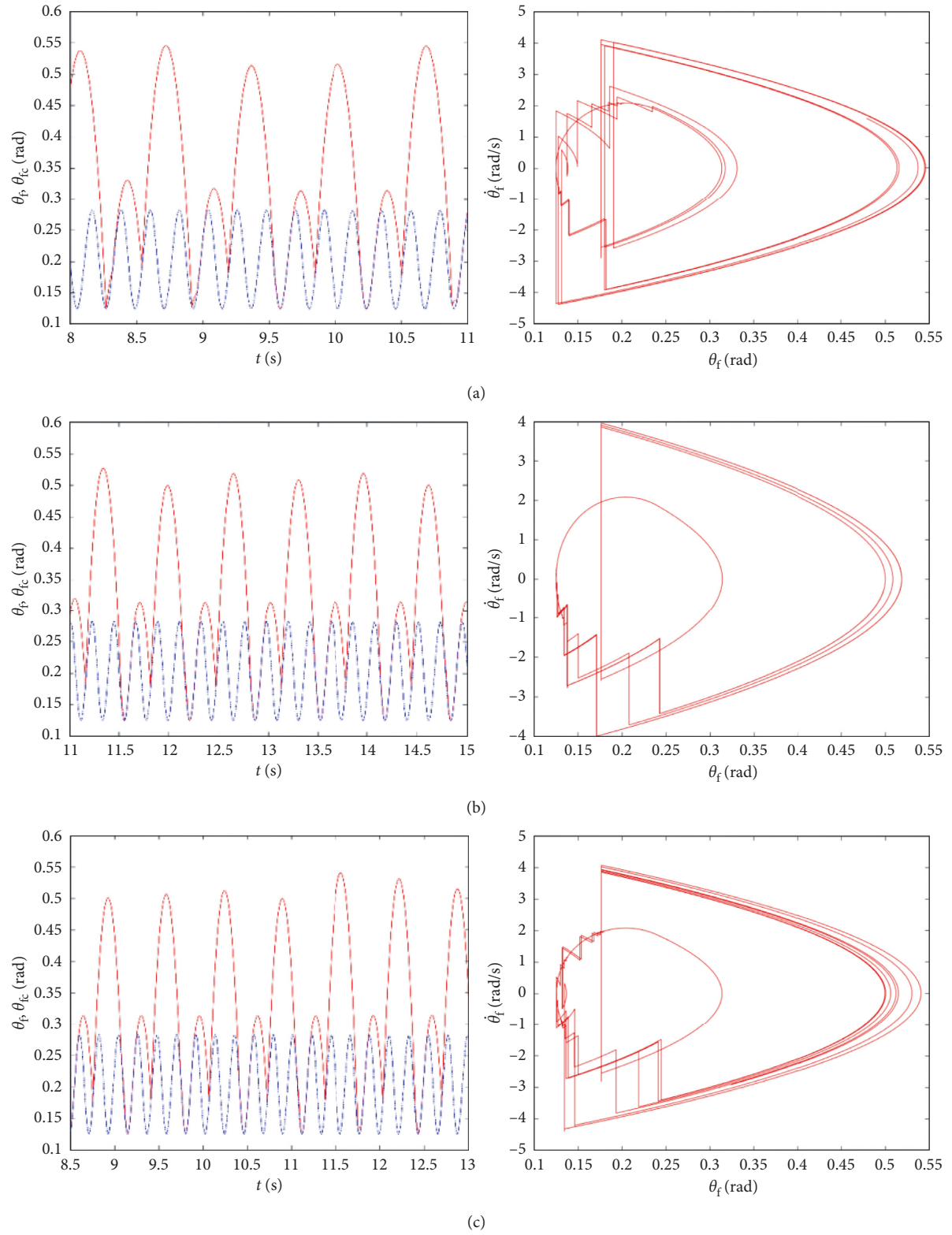

FIGURE 10: System response after applying a random deviation ($\mu = 0.023$ m). (a) Quasiperiod 2 ($\sigma = 0.001$ m; left frame: red represents θ_f, blue represents θ_{fc}). (b) Quasiperiod 2 ($\sigma = 0.002$ m; left frame: red represents θ_f, blue represents θ_{fc}). (c) Quasiperiod 2 ($\sigma = 0.003$ m; left frame: red represents θ_f, blue represents θ_{fc}).

changes as a minor parameter varies, and the system response eventually turns into chaos with the increase of D.

(3) The system response changes between quasiperiod and chaos affected by the contact line length with a normal random distribution.

Data Availability

The data used to support the findings of this study are available from the corresponding author upon request.

Conflicts of Interest

The authors declare that they have no financial or non-financial competing interest, and all of the authors agree to the publication of this paper.

Acknowledgments

This study was funded by the National Natural Science Foundation of China (grant number 11272257), NPU Aoxiang New Star and the Fundamental Research Funds for the Central Universities (grant number 3102018ZY016), and the Key Laboratory of Vibration and Control of Aero-Propulsion System Ministry of Education, Northeastern University (grant number VCAME201803).

References

[1] P. Flores, R. Leine, and C. Glocker, "Modeling and analysis of planar rigid multibody systems with translational clearance joints based on the non-smooth dynamics approach," *Multibody System Dynamics*, vol. 23, no. 2, pp. 165–190, 2009.

[2] Y. Yang, Q. Wu, Y. Wang, W. Qin, and K. Lu, "Dynamic characteristics of cracked uncertain hollow-shaft," *Mechanical Systems and Signal Processing*, 2019, In press.

[3] R. Lima and R. Sampaio, "Stick-mode duration of a dry-friction oscillator with an uncertain model," *Journal of Sound and Vibration*, vol. 353, pp. 259–271, 2015.

[4] H. Dai, X. Jing, Y. Wang, X. Yue, and J. Yuan, "Post-capture vibration suppression of spacecraft via a bio-inspired isolation system," *Mechanical Systems and Signal Processing*, vol. 105, pp. 214–240, 2018.

[5] Y. Yang, H. Chen, and T. Jiang, "Nonlinear response prediction of cracked rotor based on EMD," *Journal of the Franklin Institute*, vol. 352, no. 8, pp. 3378–3393, 2015.

[6] M. D. Nora, T. D. M. Lanzanova, and H. Zhao, "Investigation of performance and combustion characteristics of a four-valve supercharged two-stroke DI engine fuelled with gasoline and ethanol," *Fuel*, vol. 227, pp. 401–411, 2018.

[7] R. Alzate, M. di Bernardo, U. Montanaro, and S. Santini, "Experimental and numerical verification of bifurcations and chaos in cam-follower impacting systems," *Nonlinear Dynamics*, vol. 50, no. 3, pp. 409–429, 2007.

[8] Y. Shen and W. J. Stronge, "Painlevé paradox during oblique impact with friction," *European Journal of Mechanics-A/Solids*, vol. 30, no. 4, pp. 457–467, 2011.

[9] H. S. Yan, M. C. Tsai, and M. H. Hsu, "An experimental study of the effects of cam speeds on cam-follower systems," *Mechanism and Machine Theory*, vol. 31, no. 4, pp. 397–412, 1996.

[10] W. Zhang and M. Ye, "Local and global bifurcations of valve mechanism," *Nonlinear Dynamics*, vol. 6, no. 3, pp. 301–316, 1996.

[11] T. Zhang, H. G. Li, Z. Y. Zhong, and G. P. Cai, "Hysteresis model and adaptive vibration suppression for a smart beam with time delay," *Journal of Sound and Vibration*, vol. 358, pp. 35–47, 2015.

[12] H. Ding and L.-Q. Chen, "Galerkin methods for natural frequencies of high-speed axially moving beams," *Journal of Sound and Vibration*, vol. 329, no. 17, pp. 3484–3494, 2010.

[13] H. Ding, L.-Q. Chen, and S.-P. Yang, "Convergence of Galerkin truncation for dynamic response of finite beams on nonlinear foundations under a moving load," *Journal of Sound and Vibration*, vol. 331, no. 10, pp. 2426–2442, 2012.

[14] R. Alzate, M. di Bernardo, G. Giordano, G. Rea, and S. Santini, "Experimental and numerical investigation of coexistence, novel bifurcations, and chaos in a cam-follower system," *SIAM Journal on Applied Dynamical Systems*, vol. 8, no. 2, pp. 592–623, 2009.

[15] R. Alzate, P. T. Piiroinen, and M. di Bernardo, "From complete to incomplete chattering: a novel route to chaos in impacting cam-follower systems," *International Journal of Bifurcation and Chaos*, vol. 22, no. 5, article 1250102, 2012.

[16] S. Sundar, J. T. Dreyer, and R. Singh, "Rotational sliding contact dynamics in a non-linear cam-follower system as excited by a periodic motion," *Journal of Sound and Vibration*, vol. 332, no. 18, pp. 4280–4295, 2013.

[17] N. A. H. Tsuha, F. Nonato, and K. L. Cavalca, "Formulation of a reduced order model for the stiffness on elastohydrodynamic line contacts applied to cam-follower mechanism," *Mechanism and Machine Theory*, vol. 113, pp. 22–39, 2017.

[18] W. Pan, X. Li, L. Wang, N. Guo, and Z. Yang, "Influence of contact stiffness of joint surfaces on oscillation system based on the fractal theory," *Archive of Applied Mechanics*, vol. 88, no. 4, pp. 525–541, 2017.

[19] A. Majumdar and B. Bhushan, "Fractal model of elastic-plastic contact between rough surfaces," *Journal of Tribology*, vol. 113, no. 1, pp. 1–11, 1991.

[20] C. Padmanabhan and R. Singh, "Dynamics of a piecewise non-linear system subject to dual harmonic excitation using parametric continuation," *Journal of Sound and Vibration*, vol. 184, no. 5, pp. 767–799, 1995.

[21] X. Zhang, N. Wang, G. Lan, S. Wen, and Y. Chen, "Tangential damping and its dissipation factor models of joint interfaces based on fractal theory with simulations," *Journal of Tribology-Transactions of the ASME*, vol. 136, no. 1, article 011704, 2014.

[22] S. Wang and K. Komvopoulos, "A fractal theory of the interfacial temperature distribution in the slow sliding regime: Part II-multiple domains, elastoplastic contacts and applications," *Journal of Tribology*, vol. 116, no. 4, pp. 824–832, 1994.

[23] S. Wang and K. Komvopoulos, "A fractal theory of the interfacial temperature distribution in the slow sliding regime: Part I-elastic contact and heat transfer analysis," *Journal of Tribology*, vol. 116, no. 4, pp. 812–822, 1994.

[24] K. L. Johnson, *Contact Mechanics*, Cambridge University Press, Cambridge, UK, 1987.